Chemical Science

ROYAL SOCIETY OF CHEMISTRY

EDGE ARTICLE

Cite this: *Chem. Sci.*, 2021, **12**, 10930

All publication charges for this article have been paid for by the Royal Society of Chemistry

Natural products dereplication by diffusion ordered NMR spectroscopy (DOSY)†

Guy Kleks, [ab] Darren C. Holland, [ab] Joshua Porter[ab] and Anthony R. Carroll *[ab]

Diffusion-ordered NMR spectroscopy (DOSY) can be used to analyze mixtures of compounds since resonances deriving from different compounds are distinguished by their diffusion coefficients (*D*). Previously, DOSY has mostly been used for organometallic and polymer analysis, we have now applied DOSY to investigate diffusion coefficients of structurally diverse organic compounds such as natural products (NP). The experimental *D*s derived from 55 diverse NPs has allowed us to establish a power law relationship between *D* and molecular weight (MW) and therefore predict MW from experimental *D*. We have shown that *D* is also affected by factors such as hydrogen bonding, molar density and molecular shape of the compound and we have generated new models that incorporate experimentally derived variables for these factors so that more accurate predictions of MW can be calculated from experimental *D*. The recognition that multiple physicochemical properties affect *D* has allowed us to generate a polynomial equation based on multiple linear regression analysis of eight calculated physicochemical properties from 63 compounds to accurately correlate predicted *D* with experimental *D* for any known organic compound. This equation has been used to calculate predicted *D* for 217 043 compounds present in a publicly available natural product database (DEREP-NP) and to dereplicate known NPs in a mixture based on matching of experimental *D* and structural features derived from NMR analysis with predicted *D* and calculated structural features in the database. These models have been validated by the dereplication of a mixture of two known sesquiterpenes obtained from *Tasmannia xerophila* and the identification of new alkaloids from the bryozoan *Amathia lamourouxi*. These new methodologies allow the MW of compounds in mixtures to be predicted without the need for MS analysis, the dereplication of known compounds and identification of new compounds based solely on parameters derived by DOSY NMR.

Received 31st May 2021
Accepted 15th July 2021

DOI: 10.1039/d1sc02940a

rsc.li/chemical-science

Introduction

One of the challenges in natural product (NP) discovery is the re-isolation and identification of known compounds. The process of identifying these known compounds early in the discovery process is known as dereplication. Using dereplication strategies, the time consuming process involved in re-isolation and structure elucidation of known compounds is avoided allowing the isolation and structure elucidation efforts to focus solely on new compounds.[1] In NP discovery, LC-MS is a common tool for dereplication. This requires comparison of data acquired by MS or tandem MS (MS/MS) with that of known NPs found in databases. This has been facilitated by the use of molecular networking *via*, for instance, the free online community-based platform Global Natural Products Social Molecular Networking (GNPS), in which MS/MS data is used to identify a network of chemically related NPs.[2,3] Unfortunately, because fragmentation patterns, ion intensities and the experimental parameters used to acquire data can vary across instruments, mis-identification and/or failure to identify compounds can still occur.[4–6]

While the most common NP dereplication techniques are MS-based, the main tool for structure elucidation of NPs is NMR spectroscopy. The only approach currently used to correlate NMR and MS data is by hyphenated NMR techniques such as LC-NMR-MS. This technique allows real-time acquisition of combined MS and NMR data to be obtained for compounds eluting from a LC system.[7] While hyphenated NMR is a powerful tool for dereplication, it is time consuming and requires specialized and expensive hardware not available in most laboratories. An alternative approach is to perform LCMS separation first, followed by fraction analysis (after evaporation and reconstitution in an appropriate NMR solvent) either in NMR tubes or using a flow NMR probe.[8] This technique is also labour intensive and time consuming.

[a]*School of Environment and Science, Griffith University, Gold Coast, QLD 4222, Australia. E-mail: a.carroll@griffith.edu.au*

[b]*Griffith Institute for Drug Discovery, Griffith University, Brisbane, QLD 4111, Australia*

† Electronic supplementary information (ESI) available: Structures of all compounds used in the analysis, tables of data used to generate molecular weight and diffusion co-efficient predictions and figures associated with models 1, 2, 3 and 4. See DOI: 10.1039/d1sc02940a

The difference between MS and NMR gives rise to several problems:

(1) Since MS is several orders of magnitude more sensitive than NMR, compounds that are marked as potential new compounds by MS-based dereplication techniques may be present in concentrations too small for isolation and subsequent NMR identification.

(2) Compounds that are not easily ionizable may not be visible by MS. Furthermore, those with low signal intensities may be overlooked.

(3) Structural/configurational isomers can be misidentified as known compounds by MS, while NMR analysis can delineate the difference between isomers more clearly.

(4) There are approximately 30 000 unique accurate masses that account for >215 000 published NPs. However, many of these masses are represented by hundreds of different NPs. For example 264.13615 da represents the MW of 640 different NPs.[9]

These points highlight the need for more accessible NMR-based dereplication methods that allow for the identification of compounds in mixtures. Recent developments in this area include a large open access NP database that is functional group annotated for NMR feature matching (DEREP-NP),[9] a HSQC-TOCSY analysis method that has been used to identify molecular fragments in complex mixtures,[10] SMART 2.0 (Small Molecule Accurate Recognition Technology) a machine learning tool to identify compounds in mixtures based on HSQC data[11] and MADByTE (Metabolomics and Dereplication by Two-Dimensional Experiments) a tool that associates HSQC and TOCSY data from complex mixtures to allow identification of molecular networks.[12] A significant limitation of these methods is that none have the ability to predict the MWs of resonances computationally annotated by NMR.

Diffusion-ordered spectroscopy (DOSY) is an NMR technique that allows resonances associated with individual components in a mixture to be separated in the NMR tube based on their size. This non-destructive technique does not require any special equipment and can be performed on any modern NMR spectrometer.

Based on pulsed field gradient (PFG) NMR, the diffusion rate of a compound in a solvent is measured by acquiring a series of spectra at incrementing gradient strengths, resulting in signal attenuation that is used to calculate a diffusion coefficient (D). This provides a DOSY spectrum, a pseudo-2D spectrum in which the resonances are separated in a derived second dimension according to the diffusion rate of the molecule they emanate from. The diffusion of a molecule in solvent is described by the Stokes–Einstein equation as the diffusion coefficient (D):

$$D = \frac{k_b T}{6\pi\eta r_H}$$

This equation assumes a molecule possesses a sphere-like shape and is dissolved in a continuous fluid. In the numerator k_b is the Boltzmann constant and T is the temperature. The denominator represents the friction experienced by the molecule, in which η is the solvent viscosity and r_H is the hydrodynamic radius of the molecule.[13]

Differences in T between samples will result in variation of Ds and the temperature should be kept constant in order to compare Ds of different samples. Sample temperature should also be regulated, since a temperature gradient in the sample could lead to convection, resulting in erroneous Ds.[14] While low viscosity solvents, such as chloroform (0.54 cP at 298 K), are more prone to the formation of convection, DMSO is more viscous (1.99 cP at 298 K), making it a good candidate for DOSY.[14] The solvent viscosity (η) changes with sample concentration,[15] affecting the diffusion rate of all the components in the sample. To be able to compare the Ds of compounds measured in different samples, an internal reference must be used. While an obvious choice for an internal reference would be the residual NMR solvent peak, previous research has shown ambiguous results, with some advising caution with referencing Ds to the solvent signal,[15] while others have reported excellent results.[16]

The Stokes–Einstein equation states that the D of the molecule possesses an inverse relationship to its hydrodynamic radius. In other words, a small molecule diffuses faster than a large one, thereby displaying a larger D value. Therefore, DOSY provides a spectroscopic separation of the signals associated with compounds in a mixture without any physical separation, making DOSY a powerful technique for mixture analysis.

A significant limitation of DOSY is signal overlap, complicating the extraction of the D since the observed signal attenuation is derived from two or more components with different diffusion rates. While there are several techniques that attempt to resolve this problem, it remains a very complicated task.[16,17] Clearly, this poses a problem for complex mixtures such as those commonly encountered in NP research. However, DOSY can be implemented with 2D NMR experiments such as DOSY-COSY and DOSY-HSQC,[18,19] expanding the diffusion into another dimension thus minimizing the possibility of signal overlap. Alternatively, the likelihood of overlap could be reduced by collapsing all signal multiplets to singlets using pure shift DOSY.[20]

As DOSY separates the resonances in a mixture according to their D, corresponding to molecular size, the D can be correlated to molecular weight (MW). There are many examples in which DOSY was used to determine MW from D of polymers,[21,22] simple organic compounds[15] and organometallics.[14,23] However, in NP research DOSY has only been used for separation of resonances by their D, and this information was not correlated to any other physical or chemical properties. To our knowledge, there are only two examples in which DOSY has been used in NP discovery for the dereplication and identification of unknown compounds. The first was the dereplication of a chromatographically inseparable mixture of NPs from a marine cyanobacterium,[24] and while the second was used to aid in the identification of a mixture of bromopyrroles from the marine sponge *Agelas* sp.[25] Since the literature contains very little information about D of NPs, dereplication of NPs by DOSY cannot currently rely solely on experimental D. Therefore, experimentally derived D need to be investigated in more detail to determine if this property correlates to a common physical

property used for dereplication, such as MW or if it can be used as surrogate for MW.

In this paper, we investigate correlations between experimental D of NPs to various structural and chemical properties. This has allowed us to develop models that can be used to dereplicate known NPs and identify new NPs through application of DOSY NMR techniques.

Results and discussions

Referencing DOSY data

As described above, the viscosity of the NMR solvent can affect D, and changes in the concentration of dissolved analytes can affect the viscosity of the solvent. To avoid these issues we have used relative diffusivity of an internal reference compound to account for variations of viscosity between samples.[26] The "standard" D of the reference (D_{stand}) was determined as the D of the reference in a blank sample (containing only the reference compound and the NMR solvent at 350 μM), and the ratio between the observed D of the reference (D_{ref}) in each sample to that of the standard was used to standardize the D of the compound (D_{comp}) using the following equation:

$$D = \frac{D_{stand}}{D_{ref}} D_{comp}$$

This referencing method enables the DOSY data to be reproducible (Fig. S1†), allowing D values acquired for compounds to be compared even on different spectrometers using different pulse sequences. An ideal reference should resonate at a chemical shift that rarely overlaps with analyte resonance and should have a diffusion co-efficient like that of the analytes.

Since diffusion parameters in the DOSY NMR pulse sequence should be set to provide up to ~90% signal attenuation for analytes, and since the average MW of reported NPs is 414 amu,[27] we chose tetrakis(trimethylsilyloxy)silane (TTMS), 384.84 amu, D_{stand} 3.157 10^{-10} m^2 s^{-1} at 298 K as a more suitable internal reference. TTMS shows good solubility in DMSO, is a liquid at room temperature making it easy to handle, and with a boiling point of 103–106 °C, can be evaporated upon removal of DMSO (189 °C) from the sample. TTMS displays a single proton resonance at δ_H 0.09 ppm derived from its 12 constituent methyl groups (36 protons) meaning only a small concentration (0.5% v/w) is enough to produce an intense signal.

The relationship between D to MW

The relationship between D to MW is non-linear, and has been shown to possess a power-law relationship:[21]

$$D = A \times MW^{\alpha}$$

To achieve a linear relationship, the logarithms of both the D and MW should be used:

$$\log(D) = \alpha \log(MW) + \log(A) \quad (1)$$

However, it has been shown that a specific power-law relationship needs to be established for each compound class and each solvent.[28] After a correlation between D to MW is determined, it can be used to predict the MW of an unknown compound in a specific compound class from its experimental D. While this model has been shown to produce accurate MW predictions for specific compound classes,[14,23] variation between structure classes has been shown to produce large errors in MW estimation.[15,29]

We have acquired ^{1}H DOSY spectra in DMSO-d_6 for 55 individual compounds with a MW range of 123–1486 amu, including 38 NPs, four NP derivatives, and 13 synthetic compounds of which eight are drugs (Table S1,† for structures and numerical structure codes see ESI†). The NPs in the dataset consist of diverse structure classes such as oxygenated linear and cyclic terpenes, alkaloids and their TFA salts, anthracycline, a β-triketone, a coumarin derivative, a saponin, and macrocyclic compounds such as macrolide antibiotics.

The least-squares fit of the experimental log D *vs.* the log MW of each compound generated model 1 ($n = 55$, $R^2 = 0.852$) with coefficient values of −0.6057 and −8.0952 for α and log(A), respectively.

model 1:

$$MW_{pre} = 10^{((\log(D)+8.0952)/(-0.6057))}$$

To quantify the accuracy of the MW prediction (MW_{pre}), the MW_{pre} error as the percentage of the residual MW_{pre} from the true MW (MW_{true}) for each compound was determined (eqn (2)):

$$MW_{pre}\ \text{error} = (MW_{pre} - MW_{true})/MW_{true} \quad (2)$$

This provides an intuitive error scale in which compounds that diffuse slower than their predicted D (D_{pre} – derived from the calibration curve) will translate to a MW_{pre} value that is greater than their true MW and will therefore display a positive error, and underestimation of MW_{pre} will show a negative error.

In previous research, calibration curves generated using the power law relationship in $CDCl_3$ and D_2O displayed MW_{pre} errors mostly within a range of ±30%.[29] While analysis of data previously reported for compounds in THF-d_8 and toluene-d_8 (Tol-d_8) showed MW_{pre} errors within a range of ±20%.[14] Our results in DMSO-d_6 showed an average +20.6% MW_{pre} error for overestimated compounds, and −14.7% for underestimated compounds. However, the total MW_{pre} error range for our dataset was larger than for $CDCl_3$, D_2O, THF-d_8 or Tol-d_8 with a maximum error of +55% for overestimated compounds and −32% for underestimated compounds (Fig. 1).

The difference in the MW_{pre} error range observed for compounds previously studied in $CDCl_3$ and D_2O (although none of these compounds structures were disclosed in the paper)[29] compared to DMSO can be attributed to the wider dissolution range of DMSO, capable of dissolving more polar compounds than $CDCl_3$ and less polar compounds than D_2O.

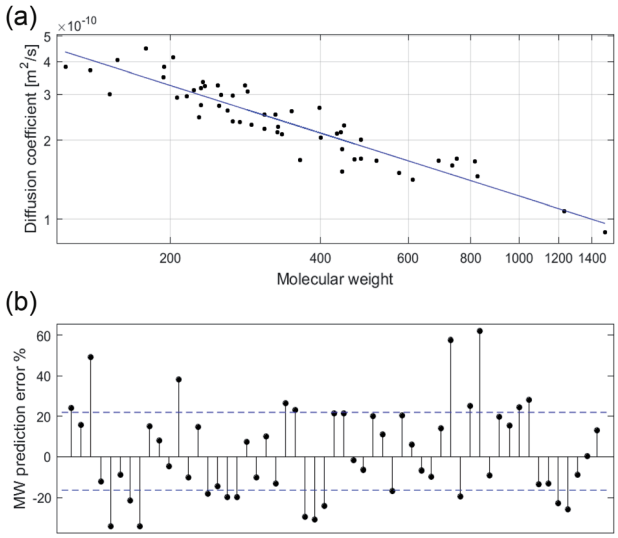

Fig. 1 log–log plot of the experimental D in DMSO-d_6 against MW for each individual compound (n = 55) (a). The residual error for each compound as percentage of MW prediction from the true MW with mean error range in blue (b).

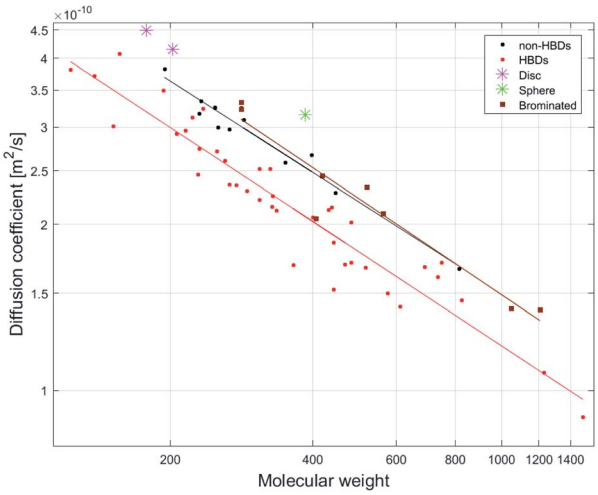

Fig. 2 Log–log plot of relationships between D to MW for three compound groups: HBD-containing compounds (n = 40, R^2 = 0.91), non-HBD containing compounds (not including disc or sphere-like compounds) (n = 13, R^2 = 0.94) and brominated compounds (n = 7, R^2 = 0.99).

All of the compounds previously studied in THF-d_8 and Tol-d_8 are lipophilic with low structural diversity.[15] In contrast, our dataset consists of structurally diverse compounds displaying a wide polarity range, with c log P ranging from −7.0 to 9.6 (see Fig. S2† for comparison of physicochemical properties). Several NPs in our dataset such as carboxylic acids, aminoglycoside and flavonoids are too polar to be dissolved in $CDCl_3$. Since the high structural diversity of the compounds used in this study to directly correlate D with MW resulted in an inaccurate power law (model 1) relationship, we next investigated the factors that contributed to these variations with the aim to establish a more accurate DOSY MW prediction model.

Molecular shape

Molecular shape affects diffusion rates with expanded disc-like (ED) or compact spherical molecules (CS) displaying faster diffusion trends relative to other molecules classified as dissipated spheres and ellipsoids (DSE).[15] Pyrene (**8**), anthracene and acridine have previously been classified as EDs.[15] Using model 1, the predicted MWs of the ED compounds **8** and phenanthrene (**5**) (Fig. 2) show significantly faster diffusion rates relative to that predicted by their MW, corresponding to a −34% MW_{pre} error for both (Fig. S3†). In addition, artemisinin (**25**), arborinine (**27**), clarithromycin (**51**) and oleandomycin-triacetate (**52**) all showed significantly faster diffusion rates than predicted by their MWs and this might also be attributed to their shape. TTMS, the reference compound for our dataset, displayed the most underestimated MW_{pre} (error of −46%) using model 1. This agreed with the literature since similar compounds, tetrakis(trimethylsilyl)silane and tris(-trimethylsilyl)amine, classified as CS display faster diffusion compared to DSE compounds.

Stalke and co-workers have suggested shape-specific MW prediction, generating power-law relationships between D and MW for three shape types: (1) CS, (2) ED and (3) DSE.[15,30] While this improved their MW prediction, for compound mixtures it requires *a priori* knowledge of the different shape-classes that are present in the mixture, reported D for these shape classes, and a method to match the resonances in the mixture with the appropriate shape class. The distinction between CS, DSE and ED shape classes is also problematic because compounds lie on a continuum between the three shape-classes. Furthermore, analogues or stereoisomers can display different hydrodynamic radii, resulting in different MW_{pre} errors within a specific shape-class and these shape-specific power law models do not work for compounds with similar shapes but containing hydrogen bond donor (HBD) or no HBD groups.

Hydrogen bonding

Intermolecular hydrogen bonding (H-bonding) can result in a slower diffusion rate than predicted by MW (*i.e.* smaller diffusion coefficient) due to an increase in the hydrodynamic radius (r_H) of the compound.[31,32] Since DMSO is a hydrogen bond acceptor (HBA), it is capable of hydrogen bonding with a hydrogen bond donor (HBD). Inspection of Fig S3† shows that most compounds with MW_{pre} errors >0 from model 1 (26 of 27) are compounds containing HBDs and those with MW_{pre} errors <0 are non-HBD containing compounds.

The effect of H-bonding on diffusion is clearly visualized by the linear least-squares fit of MW *vs.* D for HBD-containing compounds (n = 40, R^2 = 0.91) and non-HBD containing compounds (n = 13, R^2 = 0.94), as the latter display faster diffusion rates since they are not involved in H-bonding (Fig. 2).

Since the NP dataset consists of both HBD-containing compounds and non-HBD containing compounds, MW prediction using model 1 provides intermediate MW_{pre} values for these two groups. Power-law based MW prediction (*i.e.* model 1) therefore has a wide error range and will result in an

overestimated MW_{pre} for many HBD-containing compounds, and an underestimated MW_{pre} for many non-HBD containing compounds. This is demonstrated by predicting MW using model 1 for the HBD compound gemfibrozil (**19**), and the non-HBD compound parthenolide (**18**) (250.3 and 248.3 amu, respectively). Model 1 predicts MW_{pre} values that differ by 70 amu, with a MW_{pre} of 269 for **19** and a 199 MW_{pre} for **18** (Fig. S3†). Therefore, using model 1 to predict the MW for **19** from its experimental D provides an overestimated MW_{pre} of +7% (MW_{pre} error). This overestimation derives from an increase in the r_H of **19** as its HBD group is intermolecularly H-bonded to DMSO, resulting in a slower diffusion rate (smaller D). Conversely, the MW_{pre} for **18** is underestimated by −20% as it does not contain any HBDs and is therefore not involved in H-bonding with DMSO. The increase in the effective size of a compound through H-bonding with DMSO therefore relates to the equilibrium constant for the H-bonding interaction and the resident time spent as one molecular system.

Cabrita and co-workers have shown that DOSY can be used to qualitatively evaluate H-bond strength by comparing the D of HBD-containing compounds in the presence and absence of a HBA.[31,32] A HBD acidity scale (α_2^H) has been used to correlate H-bond acidity to the increase of r_H observed by DOSY for acidic compounds.[31] The α_2^H scale ranges from 0 (no H-bonding) to 1 (strongest H-bonding).[33,34] While this scale has been established in CCl_4, it has been shown that H-bond acidity ($A = \sum \alpha_2^H$) can also be predicted with high accuracy by the ^{1}H NMR chemical shift difference for a protic hydrogen between DMSO to $CDCl_3$.[35] The H-bond acidity of many classes of compounds have been determined and predictable trends relating to functional groups have been obtained. In summary, phenols, carboxylic acids, 1° amides, the amide NHs in imidazol-2-one, pyrimidine-2,4(1*H*,3*H*)-dione and related structures show comparable and strong H-bond acidity, 1° alcohols, benzylic 1° and 2° alcohols, acyclic 2° alcohols, anilides, 1° anilines, indole, pyrrole (and related aromatic amines) possess intermediate H-bond acidity, 2° anilines and 2° and 3° cyclic alcohols and vicinol diols possess weak H-bond acidity, while alkyl amines possess extremely weak H-bond acidity.[33,36] It is known that the acidity of HBD groups are also affected by factors such as electron donating or withdrawing substituents and steric hindrance and these factors also affect H-bond strength, although in many cases deviations within functional group classes are minimal.[33] Cabrita and co-workers have shown that the faster diffusion rate of 2,6-di-*tert*-butylphenol relative to its structural isomer, 2,4-di-*tert*-butylphenol, for example, is due to hindering by the second bulky group *ortho* to the phenol and this results in weaker H-bonding with the HBA.[31]

Unsurprisingly, compounds containing strongly acidic HBD groups such as carboxylic acids and phenols showed the largest MW_{pre} errors in the NP dataset when model 1 was used.

Intramolecular H-bonding between an acidic proton to an adjacent carbonyl oxygen is manifested in ^{1}H NMR spectra with the observation of the acidic proton resonating as a sharp signal at a significantly deshielded chemical shift (δ_H >12 ppm).[37] Unlike all other carboxylic acid containing compounds, nalidixic acid (**15**) displayed an underestimated MW_{pre} of −18%. This alongside a deshielded and sharp resonance at δ_H 14.89 suggested that the carboxylic acid proton is intramolecularly H-bonded and not participating in intermolecular H-bonding and this is in contrast with other compounds containing a carboxylic acid in the NP dataset. Arborinine (**27**) shows an underestimated MW_{pre} of −24% that is different to the other phenolic compounds in the dataset. A sharp and deshielded resonance at δ_H 14.86 suggests that the phenolic proton in **27** does not undergo intermolecular H-bonding because it is intramolecular H-bonded to the adjacent carbonyl oxygen. Salicylic acid (**2**) also contains an intramolecular H-bonded phenol as well as a carboxylic acid and it shows an overestimated MW_{pre} of +16% that is likely to be associated with only an H-bond between the carboxylic acid proton and DMSO.

Contribution of H-bonded DMSO to total MW

Applying the power law least squares fit equation derived from analysis of the non-HBD compounds ($n = 13$, $\alpha = -0.562$, $\log A = -8.151$, $R^2 = 0.95$) to the compounds possessing HBDs ($n = 40$) provided a predictive tool to estimate their intermolecular extended H-bonded MWs ($^{EHB}MW_{pre}$ model 1a).

model 1a:

$$^{EHB}MW_{pre} = 10^{((\log D + 8.151)/(-0.562))}$$

Subtraction of MW_{true} from $^{EHB}MW_{pre}$ and dividing this mass by the MW of DMSO-d_6 (84 amu) (eqn (3)) then allowed a good estimate of the number of intermolecular H-bonding interactions with DMSO per molecule for compounds containing functional groups with strong H-bond acidity (Fig. 3).

$$\text{Number of H-bonds} = (^{EHB}MW_{pre} - MW_{true}/MW_{DMSO\ d_6}) \quad (3)$$

Most compounds (27 out of 37) that have between one and five intermolecular HBDs based on HBD count (but excluding intramolecular H-bonds) have $^{EHB}MW_{pre}$ calculated from D within ±12% of their expected ^{EHB}MWs. This indicated that the MW errors generated by model 1 are exaggerated in small MW compounds because the mass of DMSO in one H-bonding interaction can contribute significantly to the overall mass.

Carboxylic acids

Using model 1, compounds containing a carboxylic acid as the sole intermolecular HBD group showed overestimated MW_{pre}: niacin (**1**) (+24%), **2** (+16%), ibuprofen (**9**) (15%), naproxen (**13**) (15%) and **19** (+7%). These MW_{pre} errors agree with a single DMSO H-bonding interaction and the variation in error is the result of the different mass contribution of the compound and DMSO to the overall ^{EHB}MW.

Phenols

Compounds that contain phenolic groups as the only HBD group also display overestimated MW_{pre} using model 1. While

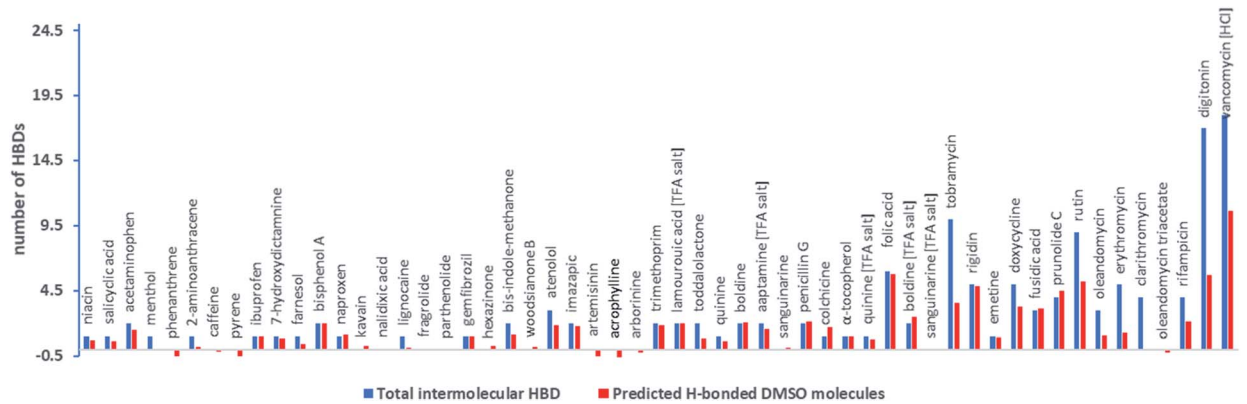

Fig. 3 Total intermolecular HBDs per compound and predicted number of DMSO molecules associated with intermolecular H-bonding interactions per molecule derived from model 1a and eqn (3).

boldine (**32**) and prunolide C (**47**) show similar overestimated MW_{pre} of +20% and +24%, bisphenol A (**12**) and 7-hydroxydictamnine (**10**) display variation in MW_{pre} error with +38% and +8% respectively. Analysis of the result from eqn (3) shows that the overestimated MW_{pre} for **47**, **32**, **12** and **10** obtained using model 1 correlates with the ratio of compound MW to number of phenols, again indicating that the magnitude of the error correlates with the mass of the combined DMSO interactions relative to the MW of the compound. The phenol, α-tocopherol (**37**), displays an underestimated MW_{pre} (−7%) using model 1 but applying eqn (3) shows that this error can still be explained by one DMSO molecule H-bonding with **37**.

Even though **37** displays a slightly lower H-bond acidity ($A = 0.43$) compared to **12** and **32** ($A = 0.48$ and $A = 0.52$ respectively), which can be attributed to steric hindrance by the adjacent methyls in the 2,6-dimethylphenol moiety, this does not significantly reduce its H-bonding interaction with DMSO.

Nitrogen HBD groups

Some compounds that contain only protons attached to nitrogen as the sole HBD group displayed less significant MW_{pre} overestimation than carboxylic acids and phenols using model 1. Penicillin G (**35**) and colchicine (**36**) both containing a secondary amide, displayed MW_{pre} errors of +21% and +6%. Analysis of the results from eqn (3) suggests that **35** has two H-bonding interactions with DMSO (*via* its carboxylic acid and amide protons) and **36** has 1.5 interactions, with the tropanone ring in **36** likely acting as a weak second HBD. Two additional compounds, imazapic (**24**) and lamouroic acid (**29**), both containing carboxylic acid and amide groups display similar MW_{pre} errors (+23% and +21%) were also predicted to have two H-bonding interactions with DMSO (based on analysis of eqn (3)). Trimethoprim (**28**), containing two 1° amines attached to a pyrimidine, displayed the largest MW_{pre} overestimate (+22% error using model 1) for a compound containing an N HBD group in the dataset however the estimated number of H-bonding interactions with DMSO (using eqn (3)) is two, as expected. Emetine (**44**), containing a secondary amine displayed an underestimated MW_{pre} of −9% and a predicted 0.8 interaction with DMSO. These results are in line with literature expectations since amides show significantly higher H-bond acidity than secondary amines.[33,34] The bis-indole, di(1*H*-indol-3-yl)methanone (**21**) displayed a MW_{pre} error of +10% but the result from eqn (3) suggests that only 1.2 DMSO molecules are predicted to H-bond to it. Likewise, 2-aminoanthracene (**6**) containing an aniline moiety had an underestimated MW_{pre} of −9% and an estimated DMSO H-bonding contribution of 0.3. These results are also in line with the predicted H-bond acidity scale since indoles are more acidic than anilines, but less acidic than amides.

Lignocaine (**16**) contains an acetanilide moiety but displays an underestimated MW_{pre} of −14% that is indicative of a non-HBD containing compound. The predicted H-bonding contribution of DMSO is also low (0.2). This does not agree with the literature as acetanilides displays high hydrogen bond acidity ($\alpha_2^H = 0.50$) compared to other nitrogen functional groups.[34] Therefore, this suggests that the amide proton is sterically hindered by the methyls of the 2,6-dimethylphenyl moiety and this conclusion is reinforced by a very low measured H-bond acidity ($A = 0.04$) for the amide proton in **16**.

Alcohol HBD groups

Of the remaining eight compounds with $^{EHB}MW_{pre}$ lower than expected all but one contains alcohols or aniline HBDs, functional groups known to possess weak H-bond acidity. Four compounds, oleandomycin (**49**), erythromycin (**50**), **51** and rifampicin (**53**) are macrocycles containing three to five alcohols that most likely take part in cross ring intramolecular H-bonding, one is a vicinal diol toddalolactone and two compounds are small MW mono-alcohols. Compounds containing sugar moieties ($n = 4$) have significantly lower $^{EHB}MW_{pre}$ and this is also in line with the literature since 1,2-diols have weak H-bond acidities resulting in H-bonding in a non-equimolar ratio with DMSO. Digitonin (**54**) for example has 17 HBDs associated with a pentasaccharide and hydroxy groups in the triterpene moiety, but it appears that an additional mass equivalent to only three DMSO molecules H-bond to this compound. These observations affirm that DOSY is a powerful

tool to quantify the extent of H-bonding between the analyte and NMR solvent and that hydrogen bond acidity contributes to the residence time for hydrogen bonding interactions (and thus the average hydrodynamic radius).

Based on these observations, classifying HBD groups into three categories: phenol/carboxylic acid HBD (OH), nitrogen HBD (NH) and alcohol HBD (aOH) provided an opportunity to predict the contribution of additional MW derived from each type of HBD group.

Multiple linear regression analysis of counts of HBDs in each compound using the three HBD categories, and predicted $^{EHB}MW_{pre}$ (model 1a) *vs.* the actual MW of the compounds established a highly predictable MW estimation ($R^2 = 0.98$, $n = 55$, model 1b) and indicated that, on average, phenol/carboxylic HBDs (OH) contribute 86.081 amu, nitrogen HBDs (NH) 44.584 amu, and alcohol HBDs (aOH) 19.44 amu per HBD to the total predicted MW (Fig. 3).

model 1b:

$$MW_{pre} = 0.932 \times 10^{EHBMW_{pre}} - 86.081 \times OH - 44.584 \times NH - 19.44 \times aOH + 21.088$$

$$MW_{pre} = 0.932 \times 10^{((\log D + 8.151)/-0.562)} - 86.081 \times OH - 44.584 \times NH - 19.44 \times aOH + 21.088$$

These results are in line with H-bond acidity trends reported in the literature for acidic, phenolic and alcoholic HBDs. The reported H-bond acidity of nitrogen HBDs are quite variable and combining all counts of nitrogen HBDs into one category produced an average prediction for the MW contribution for amides, amines and aromatic NH and sub-categorizing these groups will likely improve the MW prediction further (Fig. 4).

Molecular density

Molar density is another factor affecting diffusion rates. Stalke and co-workers have shown that compounds containing heavy atoms such as bromine and iodine display fast diffusion rates relative to their MWs.[38] The molar density of the Br atom (calculated by dividing its mass by its van der Waals volume)[15] shows a 5.2/3.4/2.8-fold higher density than C/N/O atoms respectively. The linear least-squares fit of *D vs.* MW for a group of brominated NPs ($n = 7$, $R^2 = 0.99$) displayed a different diffusion trend to other compounds in the dataset (Fig. 2). Although all of the brominated compounds contain HBDs, they show faster diffusion rates compared to non-HBD containing compounds. Calculation of the Br ratio shows that the compounds that displayed fast diffusion rates possess a Br ratio >28%. The exception was botryllamide C (**56**), displaying a diffusion rate like that of other HBDs molecules (MW_{pre} error of +6%) due to a lower Br ratio of 20% (and was therefore excluded from the linear least-squares fit displayed in Fig. 2).

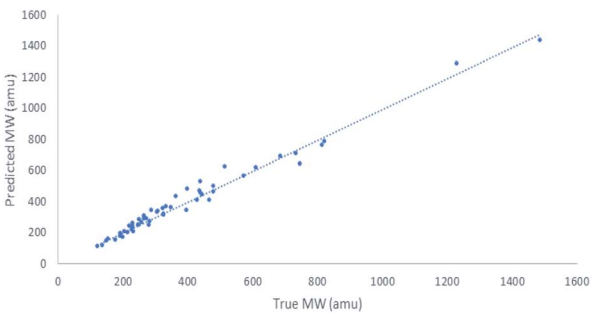

Fig. 4 Plot of relationships between MW_{true} and MW_{pre} based on model 1b with factors for acidic OH (phenols/carboxylic acids), nitrogen HBDs and alcoholic HBDs that contribute to hydrodynamic radii used to predict MW of 55 natural products and their derivatives. ($n = 55$, $R^2 = 0.98$) based on their diffusion co-efficients.

Although we did not use the brominated compounds to construct the calibration curve for model 1, the effect of bromine density on diffusion is demonstrated by comparing the MW_{pre} errors generated by applying model 1 to brominated analogues of compounds in the NP dataset. While **21** showed a MW_{pre} error of +10% due to H-bonding, its 6,6′-dibromo analogue showed a faster diffusion rate that translated to a MW_{pre} error of −24%. **47** displayed a MW_{pre} error of +24%, while its brominated analogues prunolide B (**59**) (containing 6 bromines) and prunolide A (**60**) (containing 8 bromines) displayed MW_{pre} errors of −24% and −34% respectively (Fig. S3†). The faster diffusion rate of **60** correlates to the increase in bromine ratio for **60** compared to **59** (45.8% and 53.0%), suggesting that a higher bromine ratio will result in a faster diffusion rate relative to MW, corresponding to an underestimation in MW_{pre} using model 1.

While the Br atom is significantly denser than the C atom (5.2-fold), more common elements in NPs, such as O and N, are only 1.9 and 1.5-fold denser than C. Neufeld and Stalke suggested measuring the density of a compound by dividing its MW by the sum of all van der Waals volumes of the atoms.[15] This however provided a poor correlation for the non-HBD containing compounds in our dataset due to the fact that the variation in diffusion rates relative to MW derive also from molecular shape and not just from molar density. The β-triketone woodsianone B (**22**) for example,[39] has a higher O content (24%) compared to fragrolide (**17**) and **18** (19%) and slightly lower O content than **25** but displayed a slower diffusion rate relative to its MW as it has a different molecular shape. The structurally related compounds, the sesquiterpenes **17**, **18** and **25** displayed an opposite trend. While **17** and **18** (both containing 19% O) displayed a MW_{pre} error of −20%, **25** (28% O) showed a much larger MW_{pre} error of −30%. However, this difference might also be associated with a more compact spherical shape of **25**.

A clear example where an increase in molar density is observed is for the TFA salts of alkaloids. Ion pairing is observed by DOSY as a decrease in diffusion rate (smaller *D*) as a result of an increase in the r_H of the compound.[40] Our dataset contain three alkaloids (quinine (**31**), **32** and sanguinarine (**34**)) that displayed an increased diffusion rate as TFA salts relative to their MWs (including 114 amu for TFA) compared to diffusion rates of these compounds without TFA. This increase in diffusion rate, corresponding to underestimation in MW_{pre} by model 1, indicates an increase in molar density as TFA contributes two

oxygens and three fluorines to the overall density of the compound.

While Stalke and co-workers have suggested that molar density has a larger impact on diffusion rate than molecular shape,[38] the ED compounds in our dataset, **8** and **5**, showed larger MW_{pre} errors using model 1 than brominated compounds. However, unlike in the Stalke dataset in which the majority of compounds did not contain HBDs (57 of 60),[38] all of the brominated compounds in our dataset contained at least one HBD suggesting that higher molar density counterbalances the effect of H-bonding in predicting MW. This suggests that the factors affecting MW prediction involve a combination of H-bonding, molar density and molecular shape. The correlations observed between *D* to MW for each separate group of compounds (HBDs, non-HBDs and brominated) in our dataset are more accurate than the combined relationship of HBDs and non-HBDs ($n = 55$, $R^2 = 0.85$) and therefore predicting MW from *D* for each specific HBD, non-HBD and high density compound groups is advisable. However, unless there is a method to associate the resonances observed in a mixture with compounds that do or do not contain HBDs and/or heavy atoms such as bromine then these MW prediction equations are irrelevant. For non-halogenated compounds our analysis indicates that H-bonding generates the greatest error for MW prediction by DOSY in DMSO.

Improved MW prediction models

Model 2 – hydrogen bonding observed by ^{1}H NMR. Although molecular shape and molar density can affect rates of diffusion, it is difficult to identify NMR signals that can be used to definitively assign molecular shape or molar density features in a molecule. Conversely, we have shown that HBD significantly affects *D* and acidic protons associated with HBD functional groups can be visualized by ^{1}H NMR spectroscopy as deshielded resonances (and by their exchange with D_2O) thus providing a potential tool to investigate the relationship between H-bonding, MW and *D*. Since the chemical shift of acidic protons have been shown to correlate with H-bond acidity the relationship between the chemical shift ($^{eff}\delta_H$) of the most acidic exchangeable proton observed in the ^{1}H NMR spectrum may directly correlate with the *D* of the compound.

As discussed earlier, intramolecular H-bonded protons are characteristically deshielded, resonating at frequencies greater than δ_H 12 ppm and do not usually contribute to intermolecular H-bonding. The compounds **15** and **27** display very deshielded ($>\delta_H$ 14.00) and sharp resonances that are clear indicators of intramolecular H-bonding. Therefore, in developing a HBD model, we have set an upper limit for the chemical shift of the $^{eff}\delta_H$ parameter so that only the chemical shifts of intermolecularly H-bonded protons are used. This ideally meant that the $^{eff}\delta_H$ parameter only captures HBD's that lead to an increase in a compound's r_H, and therefore affect diffusion. Since not all NPs contain HBDs, a value of $^{eff}\delta_H = 0.00$ has been set for compounds containing no HBDs. Therefore, $^{eff}\delta_H$ was limited to a chemical shifts range between 0 and 14, where $^{eff}\delta_H$ equals the most deshielded exchangeable proton resonance observed between δ_H 0 and 14.

Multiple linear regression analysis of 55 compounds afforded the following relationship:

model 2:

$$\log D = -0.6077 \log \mathrm{MW} - 0.0102\ {}^{eff}\delta_H - 8.0282$$

This model displayed a very significant improvement ($R^2 = 0.95$) in MW prediction relative to a simple power-law relationship of *D vs.* MW using model 1 ($n = 55$, $R^2 = 0.85$) (Fig S4 and S5†). The $^{eff}\delta_H$ parameter showed an excellent correlation (*P*-value $= 1.3\ 10^{-13}$) to the variation between log *D vs.* log MW.

The $^{eff}\delta_H$ parameter in model 2 is a surrogate for the MW of DMSO in the extended MW of HBD compounds. The more deshielded the exchangeable signal, the greater the mass that is subtracted from the total MW_{pre}, resulting in the MW_{pre} being closer to that expected for the MW of a compound alone (without a contribution of DMSO in HBD/HBA interactions). When the $^{eff}\delta_H$ parameter is set to 0 for any compound, the resulting MWpre are almost identical to the $^{EHB}MW_{pre}$ generated using model 1a. Model 2 improved the MW_{pre} for the polar carboxylic acids **1**, **24** and **2** displaying a very accurate MW_{pre} (−4%, −1% and −3% error compared to +24% + 23% and +16% respectively from model 1). However, only two of three lipophilic carboxylic acids **9**, gemfibrozil (**19**) and **13** had improved MW_{pre} with model 2 *vs.* model 1 (−7% *vs.* +15%, −8% *vs.* +15%, −13% *vs.* +7% respectively). Some compounds containing more than one strong HDB (such as bis phenol A, acetaminophen (**3**), atenolol (**23**), **28** and folic acid (**39**)) had improved MW_{pre} but were still >20% in error while tobramycin (**42**) and fusidic acid (**46**) had MW_{pre} errors increased to >20%. This suggested that using the exchangeable proton chemical shift of only the most deshielded resonance in the model ignored the contribution of other strongly acidic HBDs.

The amide proton in **16** is deshielded leading to a significant reduction in its MW_{pre} using model 2. This led to a MW_{pre} error for **16** of −23% (an increased underestimation of its MW_{pre} compared to model 1). The chemical shift of the NH proton does not account for the steric hindrance it experiences from the two *ortho* methyl groups.

While this model displays a very good correlation between the chemical shift of acidic exchangeable protons and variations in diffusion, it has some significant practical limitations. First, chemical exchange causes signal broadening. Resonances associated with acidic protons such as those present in carboxylic acids or phenols can undergo chemical exchange with residual H_2O, resulting in signal broadening up to a point where these resonances cannot be seen in a ^{1}H NMR spectrum. Second, several compounds in our dataset (doxycycline hyclate (**45**) **53** and rutin (**48**)) displayed resonances for intramolecular H-bonded phenols below the $^{eff}\delta_H$ limit of 14.00 ppm (δ_H 11.48, 12.44 and 12.60 ppm respectively). These intramolecular H-bonded phenolic resonances are identifiable as they are sharper than other phenols in their spectra that can undergo chemical exchange with H_2O. Third, a proton which is a HBD can undergo chemical exchange with H_2O and will display a larger *D* value than the other proton resonances in the same

compound.[41] These exchangeable proton resonances therefore display an average D value somewhere between that of the compound and that of H_2O and this D is dependent on the diffusion delay used in the pulse sequence.[41] These caveats could make it difficult to distinguish exchangeable proton resonances from specific molecules in a mixture.

Unfortunately, practical application of model 2 for MW prediction of compounds in mixtures requires the $^{eff}\delta_H$ for each compound in the mixture to be quantified. Using model 2 with a mixture containing a compound capable of intermolecular H-bonding and a compound that cannot, will significantly increase the MW_{pre} error for one of these compounds. For example, assuming a mixture contains a flavonoid and a non-polar terpene and setting $^{eff}\delta_H$ to match the exchangeable chemical shift of the phenol would decrease the MW_{pre} error for the flavonoid but increase the terpene's MW_{pre} substantially, and *vice versa*.

Therefore, application of model 2 is only applicable to mixtures that have undergone initial partitioning, such as an acid/base extraction to obtain separate fractions containing either acidic, neutral, or basic components from an extract. Alternatively, if exchangeable proton resonances observed in the spectrum of mixtures can be associated to specific groups of other resonances in the mixture based on integral intensities then different $^{eff}\delta_H$ values can be applied to each group of resonance at specific experimental D.

Model 3 – lipophilicity by RP HPLC. In modern NP drug discovery, fraction libraries are routinely generated from crude extracts for high-throughput screening, with reversed-phase HPLC (RP HPLC) used as a common method to generate such fractions.[42] The retention time of a compound derived from RP HPLC is a function of its hydrophobicity, and therefore several methods have been developed to determine compound lipophilicity by RP HPLC.[43,44] We therefore examined if lipophilicity correlates with D. Since log P is a common parameter to measure lipophilicity, we examined the correlation between D and calculated log P ($n = 55$, $R^2 = 0.870$). This was an improvement from model 1 ($n = 55$, $R^2 = 0.852$), and the P-value for calculated log P (0.009) implied a correlation to D (Table S4†). We therefore examined the correlation between the RP HPLC retention of compounds in our dataset to their D. While RP HPLC elution *vs.* % MeCN has been used to predict log P with good accuracy,[43,44] since MeOH is a much more common solvent used for RP HPLC separation of NPs we therefore investigated the relationship between D and NP elution using H_2O/MeOH gradients on C_{18} silica gel.

The % MeOH elution of 41 compounds were measured by positive or negative ESI LC-MS with a H_2O (10 mM ammonium acetate)/MeOH gradient. The dwell time was subtracted from the retention time to calculate the % MeOH at which each compound eluted. Multiple linear regression analysis using the % MeOH elution for 41 compounds has provided the following relationship:

model 3:

$$\log D = -0.6497 \log \mathrm{MW} + 0.1906\ (\%\ \mathrm{MeOH}) - 8.0979$$

This model displayed a significant improvement in MW prediction ($R^2 = 0.91$) relative to the power-law MW prediction for the same compounds ($n = 41$, $R^2 = 0.84$). The % MeOH at which compounds eluted by RP HPLC also showed a much better correlation to D (P-value $= 2.2 \times 10^{-6}$) than calculated log P (P-value $= 0.009$) for the same compounds (Fig. S6†).

In general, model 3 reduced the MW_{pre} error compared to results from model 1 for non HBD compounds as well as many of the compounds that contained a higher proportion of HBD groups relative to their MW. Most compounds containing no HBDs still have underestimated MW_{pre} while a smaller proportion of compounds containing HBD still had overestimated MW_{pre}. This suggested that the % MeOH parameter partially accounted for the MW contribution of DMSO for many HBD containing compounds leading to a reduction in the difference in the log A term in the power law relationship for compounds containing no HBDs compared to HBD compounds. The % MeOH term in model 3 is therefore a surrogate for the contribution of H-bonded DMSO to the NPs hydrodynamic radius and thus MW_{pre}. As the proportion of % MeOH required to elute a NP by RP HPLC increases, the reduction in DMSO MW contribution to MW_{pre} for HBD compounds decreases. Unfortunately, this meant that for compounds containing mainly lipophilic moieties but also containing a HBD group, and that interact with C_{18} solely through hydrophobic interactions, thus eluting in a high proportion of MeOH, the % MeOH term in model 3 does not provide a compensatory factor to reduce the MW contribution of DMSO to the overall MW_{pre} for these compounds.

Model 3 improved the MW_{pre} for the polar acids **1**, **2** and **24** displaying a MW_{pre} errors of −9%, −6% and −3% respectively. It also improved the MW prediction for **3**, **28**, **23**, **30**, **31**, **32**, **36**, **44**, **50**, **48** and **53**. However, the lipophilic acids (**9**, **19** and **13**), phenols (**37**, **47**, **10** and **12**) and **21** (eluting at 68%, 57% 78%, 100%, 64%, 62%, 67% and 63% MeOH respectively) each displayed an increased MW_{pre} error (+25%, +22% + 24%, +21%, 22%, 13%, 46% and 14% respectively). This suggested that model 3 was ineffective at improving the MW_{pre} for lipophilic compounds with a strongly acidic HBD group. Model 3 significantly improved the MW_{pre} error for **16** (−5%) suggesting that the sterically hindered amide proton does not contribute to polar interactions with the HPLC solvent (Fig. S6†).

Model 3 therefore provides a compromise MW prediction between HBD and non HBD containing compounds. It is important to note that this model is not suitable for RP HPLC fractions obtained using a H_2O/MeOH gradient with an acid modifier since the retention times of acidic and/or basic compounds will change at low pH.[43]

Predicting D by compound structural properties

The complexity of physicochemical properties that contribute to D in highly functionalised molecules such as NPs led us to the conclusion that one predictive model to correlate D with MW for complex mixtures of NPs was futile. However, through the generation of models 2 and 3 we have clearly demonstrated that with some prior knowledge of a molecular structure, accurate

predictions of D can be made. Some failings were also recognized, with molecular shape or molar density proving to be contributing factors to D as we observed for brominated compounds. Since the aim of this study is to develop an orthogonal NMR dereplication method that can correlate structural information derived from NMR with MW, we decided to see if D could be predicted based on structural features and use experimental D as a surrogate for MW. There are several public and proprietary databases that contain structures of published NPs and cheminformatics platforms provide tools to calculate a multitude of parameters that could be used to aid in the prediction of D. We have previously used the universal natural product database UNPD (containing 217 043 publicly available NPs reported prior to 2013) to develop a platform (DEREP-NP) for rapid identification of known NPs based on structural features derived from experimental MS and NMR data.[9] DEREP-NP was established in DataWarrior,[45] an open-source software that also allows other structural and chemical properties for compounds to be calculated. Based on our observations of factors that contribute to predicting accurate D, we calculated seven additional properties for all 217 049 compounds in the database. These properties accounted for:

(a) molar density through a count of oxygens which are not attached to hydrogens (heavy O), and by a Br ratio (% Br) which is calculated as the sum of the Br atoms mass as a % of the total compound MW.

(b) Molecular shape Index (shape), generated by DataWarrior, provides values close to 0 for spherical compounds and values close to 1 for linear compounds, thus taking molecular shape into account.

(c) Lipophilicity by the relative polar surface area (polarity), providing a much better correlation than c log P.

(d) Intermolecular H-bonding generated as the total mass (17 amu × tally of free phenols and carboxylic acids) as a % of total compound MW (% OH). Counts of free phenols and carboxylic acids were generated by subtracting counts of phenols and carboxylic acids that were intramolecularly H-bonded (as determined using substructure count feature). The ratio of nitrogen HBDs (% NHBD) and alcohol HBDs (% AHBD) were calculated in the same manner.

Multiple linear regression analysis of eight structural and chemical properties for the 63 compounds that we have acquired experimental D has provided the following relationship:

model 4:

$$\log D = -7.6365 - 0.7403 \log \mathrm{MW} + 0.139\ \mathrm{shape} + 0.0069\ \mathrm{heavy\ O} - 0.8506\ (\%\ \mathrm{phenol/acid}) - 0.2586\ (\%\ \mathrm{Br}) - 0.4016\ (\%\ \mathrm{NHBD}) - 0.0947 \times (\%\ \mathrm{AHBD}) - 0.1282\ \mathrm{polarity}$$

This model provides a very accurate prediction of diffusion coefficients ($n = 63$, $R^2 = 0.99$), with predicted D (D_{pre}) displaying a small average error range of −3.7% to +3.0% from experimental D, and a maximum error range of −9.3% to +7.9% (Fig. 5 and S7†).

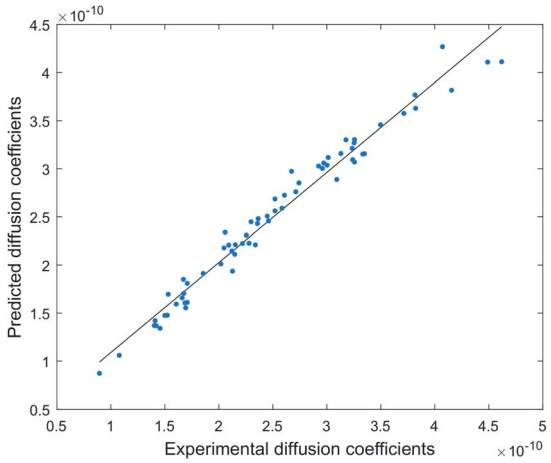

Fig. 5 Correlation between experimental and predicted diffusion coefficients ($n = 63$, $R^2 = 0.99$).

This model can be used to predict diffusion coefficients (D_{pre}) for any compound in the DEREP-NP database (or for any other database of compounds) in DataWarrior‡ and with the structural fragment tools already embedded in DEREP-NP this orthogonal D_{pre} data can replace MW data for structure matching. The histograms for counts of log(MW) and log(D_{pre}) were also very similar (Fig. 6). This again highlights the role of H-bond acceptors interacting with the DMSO solvent.

In addition, counts of the total number of basic N in a molecule allowed us to predict D ($D_{\mathrm{pre\_TFA}}$) for TFA salts of all alkaloids in the NP-DEREP database.

This is a different approach to use DOSY-based dereplication than that suggested with models 2 and 3 as the D obtained experimentally are compared against computationally predicted D_{pre}. This provides a useful tool for dereplication, allowing a D_{pre} filter based on the experimental D to be used in conjunction with other structural filters (such as counts of methyl, sp^2 proton *etc*) derived from the observed proton

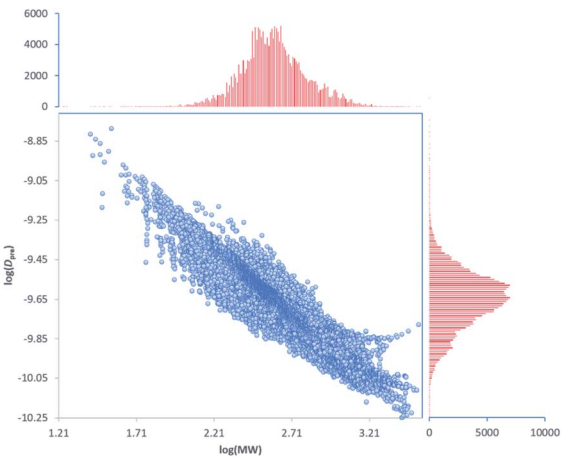

Fig. 6 Correlation between log(D_{pre}) *vs.* log(MW) and histograms of counts of log(D_{pre}) and log(MW) for all 217 043 compounds in the DEREP-NP database.

resonances in the ^{1}H NMR spectrum. We compared the D_{pre} parameter to experimental D (D_{exp}) for an additional four NPs not used in the generation of the model. The TFA salts of aerophobin-2 (**64**), 19-bromoisoeudistomin U (**65**), and aplysamine 2 (**66**) all have D_{pre} within 4% error of their experimental D, while aerothionin (**67**) had a 9% error.

Validation of models

The accuracy of models 1–4 was tested on a mixture of chromatographically inseparable compounds obtained from the Australian shrub *Tasmannia xerophila*, also known as Alpine Pepper. The ground leaf material of *T. xerophila* was extracted with MeOH and CH_2Cl_2, both fractions were combined and separated by RP HPLC and NP HPLC.

The RP HPLC fractions from *T. xerophila* was found to contained complex mixtures. Analysis of the residuals from the monoexponential fitting of the ^{1}H DOSY data showed a curvature pattern for all residuals in the δ_H 0.50–7.50 region, indicating signal decay deriving from more than one component.[16] This overlap is the major limitation of ^{1}H DOSY experiments, rendering inaccurate D values. Individual D values for overlapping resonances can potentially be extracted using multiexponential processing, however this method cannot distinguish similar D.[16] The multiexponential fitting of the ^{1}H DOSY data for the RP HPLC fraction did not result in any improvement, leading to erroneous D for resonances in the δ_H 0.50–7.50 region.

Baseline interference can be detected prior to acquiring ^{1}H DOSY data through examining the ^{1}H NMR spectrum baseline at high signal intensity. In the case of the RP HPLC fractions (Fig. S8†) there was an uneven broad baseline suggesting that the fractions contained mixtures of larger molecular weight tannins as well as small molecules. To analyze complex mixtures such as this requires a 3D DOSY methodology and this is outside of the scope of this manuscript.

The NP HPLC fractions on the other hand had a cleaner baseline, devoid of tannin signals responsible for the broad baseline. Fraction 10 (F10) predominately contained ^{1}H NMR resonances associated with a mixture of two compounds (**i**, and **ii**) in a ratio of 2 : 1 that coeluted in 70% MeOH by RP HPLC. ^{1}H DOSY data separated these resonances into two bands in the diffusion dimension (Table 1). Applying the power-law MW prediction (model 1) to this data established MW_{pre} = 160 and 185 amu for **i**, and **ii** respectively (Table 1 and Fig. 7). The ^{1}H NMR spectrum of the mixture contained a resonance for an exchangeable proton at δ_H 3.95 that, based on its integral size, could be assigned to compound (**ii**). Therefore, applying MW prediction using model 2 with $^{eff}\delta_H$ values of 0 for **i** and 3.95 for **ii** generated MW_{pre} = 202 and 202 amu for **i** and **ii** respectively (Table 1 and Fig. 7).

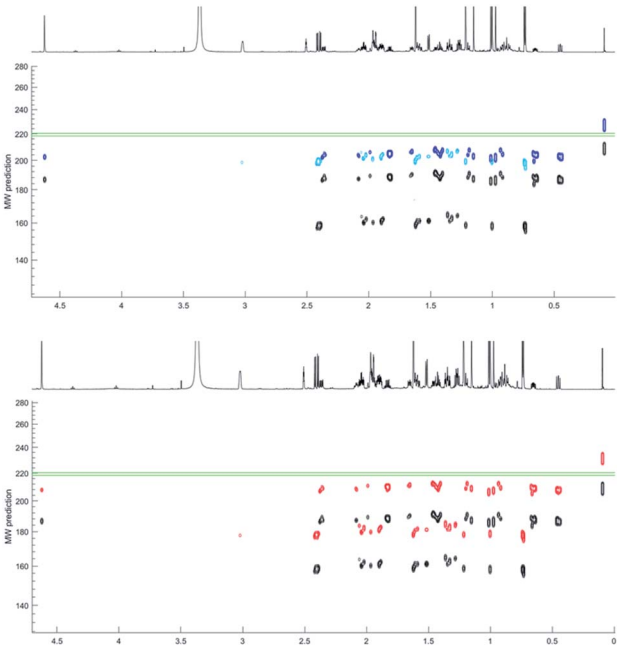

Fig. 7 MW prediction improvement with model 2 (upper blue) and model 3 (bottom red) compared to model 1 (both black) for **i** (faster diffusing) and **ii** (slower diffusing). Green lines represent true MWs.

Since the two compounds eluted with 70% MeOH by RP HPLC model 3 predicted an average MW_{pre} = 180, and 207 amu for **i**, and **ii** respectively (Table 1 and Fig. 7).

Matching D_{pre} in the DEREP-NP database to D_{exp} (±5% error) for **i** generated 4612 hits. Since DEREP-NP was specifically

Table 1 Diffusion coefficients, MW predictions and DEREP-NP hit rates for isolated NPs

	D_{exp}	D_{pre} (% error)	MW amu (% error)				DEREP-NP hits[b]		
Compound name	(10^{-10} m^2 s^{-1})		True	Model 1	Model 2	Model 3	D_{pre}[c] (±5%)	NMR/D_{pre}[d]	NMR[e]
Spathulenol (**68**)	3.40	3.55 (+4.6)	220	185 (−16)	202 (−8)	207 (−6)	8089	24	914
Cyclocolorenone (**69**)	3.72	3.70 (−0.6)	218	160 (−27)	202 (−7)	180 (−18)	4612	8	64
Convolutamine K (**70**)	2.65	2.76 (+4.1)	408	280 (−31)	353 (−13)		22 460	0	1
Convolutamine K[a] (**71**)	1.96	1.94 (−0.8)	636	460 (−28)	580 (−9)		26 470	0	1
Convolutamine L (**72**)	3.26	3.44 (+5.4)	323	198 (−39)	250 (−23)		9817	0	4
Convolutamine L[a] (**73**)	2.51	2.63 (+4.8)	437	306 (−30)	386 (−12)		23 272	0	4
Volutamine F (**74**)	1.77	1.70 (−4.1)	828	542 (−35)	683 (−18)		19 792	0	0

[a] TFA salt. [b] DEREP-NP hit compounds obtained using. [c] Only D_{pre} set to ±5% of D_{exp}. [d] Combination of NMR features and D_{pre} set to ±5% of D_{exp}. [e] Only NMR features.

developed as a tool to identify compounds based on NMR features, the additional structural features identified for the faster diffusing compound (**i**) in the ^{1}H and DOSY NMR spectra included four methyls, a methyl doublet (CH_3–CH) two methyl singlets (CH_3–Cq) and a deshielded methyl (CH_3–C sp^2), and incorporating these features as structural filters reduced the number of potential structures to 96. A pair of aliphatic protons with a large mutual 18.5 Hz coupling constant, suggesting a methylene group adjacent to a carbonyl, was present in the molecule, and a CO filter was added reducing the number of hits to 28. Since no protonated sp^2 hybridized proton was observed, setting a non-aromatic CH sp^2 filter to zero further reduced the number of hit structures to eight.

For **ii**, the D_{pre} ($\pm$5% D_{exp}) filter resulted in 8089 hit structures. Other structural filters were then applied based on the observed proton resonances: CH_3-Cq for 3 methyl singlets, zero CH sp^2 hybridized protons, >3 CH sp^3 hybridized protons and a sp^2 hybridized CH_2 group and a OH, reducing the number of hit structures to 24.

To verify the accuracy of the MW prediction generated by the four models the structures associated with the two diffusion bands of resonance were identified from analysis of 2D NMR data, to be the known sesquiterpenes spathulenol (**ii** = 68) (MW 220.35) first isolated from *Eucalyptus spathulata*,[46] and cyclocolorenone (**i** = 69) (MW 218.33) first isolated from *Pseudowintera colorata*.[47]

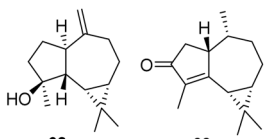

The hydroxyl proton in **68** shows H-bonding with DMSO leading to slower diffusion compared to **69** even though the two compounds have almost identical MW. Each of these compounds were present in the respective hits identified through the DEREP-NP database search. Of the eight hits matched to **i** three are **69** or its stereoisomer, while five of the 24 possible matched structures for the slower diffusing compound are **68** or its configurational isomers. For both compounds all other matches are sesquiterpenes with molecular weights $\pm$16 amu. Keeping the structural filters determined by ^{1}H NMR but eliminating the D_{pre} filter ($\pm$5% error range) increases the number of possible structures for **i** from eight to 64, and for **ii** from 24 to 914 (Table 1), demonstrating the potential of this method for dereplication. Clearly, acquiring a quick 2D experiment, such as an edited HSQC, which provides more structural information, would help to further reduce the number of hits and this approach should be considered as a possible extension for ^{1}H DOSY-based dereplication. To our knowledge, this is the first database to contain predicted *D* data for compounds.

This real-life example validates that models 2 and 3 more accurately predict MWs than a power-law model (Table 1). H-bonding contributes to the variation in *D* relative to MW, providing a clear separation in the diffusion dimension for two compounds with only a 2 amu difference in MW. We have recently published the structures of several new brominated alkaloids isolated from the bryozoan *Amathia lamourouxi*.[48] To further test the application of this dereplication methodology, we acquired DOSY data for both the free bases and TFA salts of (**70** and **71**) and K (**72** and **73**) and the free base of volutamine F (**74**). Their D_{pre} *vs.* D_{exp} were all within 5.5% error. Applying the D_{pre} filter ($\pm$5%) in DEREP-NP and adding filters for counts of aromatic singlets, aromatic methoxys and *N*-methyls produced no hits indicating that the compounds were not, as expected, in the database and were thus considered to be new.

Conclusions

The quest to develop a tool to predict MW by NMR has ultimately led us to produce a highly accurate model to predict diffusion coefficients based on structural features. Experimental *D* can be correlated to predicted *D* (a surrogate for MW) and this orthogonal physicochemical property along with structural features, both of which are derived from NMR can be used to dereplicate known structures found in databases without the need to acquire mass spectroscopic data. Furthermore, the acquisition of *D* for compounds in mixtures can be used as a tool to identify new compounds. Recently developed tools such as SMART 2.0 (ref. 11) and MADByTE[42] that use 2D NMR data derived from mixtures to dereplicate or predict structures in databases will significantly benefit from an orthogonal tool to correlate predicted *D* with experimentally derived *D* (a surrogate for MW). This DOSY methodology is highly applicable to areas outside of NP research and could be adapted more broadly in metabolomics and lipidomics research. We are currently investigating potential to apply the DOSY diffusion coefficient prediction tool to 3D NMR data such as DOSY-COSY and DOSY-HSQC for molecular network matching.

Experimental

LC-MS analysis was carried out on an Agilent 6530 Q-TOF mass spectrometer with a 1200 Series autosampler and 1290 Infinity LC module using electrospray ionization with a mobile phase linear gradient of 100% H_2O (10 mM ammonium acetate) to 100% MeOH on a Kinetex® 5 μm C_{18} 100 Å (100 × 4.60 mm) column over 10 min. Each compound was injected individually, and retention times were determined in (+) or (−) mode and by UV. The total dwell time of the system was measured by UV and was found to be 1.2 min, this was then subtracted from the retention times of compounds and divided by the total number of mins to afford the % MeOH at which each compound eluted. HPLC separation was performed on a Merck Hitachi L-7100 pump equipped with a L-7455 diode array detector, and fractions were collected with a Gilson 215 liquid handler. The total dwell time of HPLC system was determined to be 3.7 min by UV measurement. The solvents used for HPLC separation were HPLC grade, and solvent used for LC-MS analysis were LC-MS grade. H_2O was filtered using a Millipore Milli-Q PF.

NMR data was recorded at 298 K on a Bruker Avance III HDX 800 MHz spectrometer with a triple resonance 5 mm cryoprobe,

and a Bruker III 500 MHz spectrometer with a 5 mm probe. All compounds were prepared as individual samples in 3 mm NMR tubes with 200 μL of DMSO-d_6 with 0.5% (v/v%) TTMS. The ^{1}H DOSY data was acquired without sample spinning at 298 K. The pulse sequence used was LEDBP (*ledbpgp2s* in the Bruker library) with 32 768 data points and 32 scans. The diffusion delay (Δ) was kept constant at 0.1 s and the diffusion pulse (δ) was adjusted to provide ~90% signal attenuation for each compound, the spoil gradient was 0.6 ms, the gradient recovery delay was 0.2 ms and the eddy current delay was 5 ms. Each experiment was acquired with 24–32 diffusion gradients incremented linearly from 5 to 95% of the maximum gradient strength.

NMR data was processed in TopSpin 3.6.1, without zero-filling and with line broadening of 0.3–0.5 Hz. The 2D DOSY spectra were generated with Dynamics Center 2.5.2 using monoexponential curve fitting. The D for each compound was calculated as the average D of all signals that showed accurate D without any signal overlap. The average D for a compound was referenced to TTMS signal at 3.157×10^{-10} m^2 s^{-1}, which was determined from a mixture of only TTMS and DMSO in three different samples.

All calculations were carried out using MATLAB 2016a (The MathWorks, Inc.). The log P calculation and parameters used to establish model 4 were generated in OSIRIS DataWarrior Version 5.2.1 by adding substructure counts to the DEREP-NP database. D_{pre} and $D_{pre\ TFA}$ were generated by applying the formula from model 4 using the "calculated values" function in DataWarrior.

The *Tasmannia xerophila* plants were purchased from Victorian Alps Nursery, Victoria, Australia. The dried and ground *T. xerophila* leaf material (80 g) was exhaustively extracted with CH_2Cl_2 and MeOH, collectively yielding a dark green gum (16 g). The combined extracts were dissolved in MeOH and adsorbed onto C_{18} silica and loaded to an HPLC cartridge (20 mm × 10 mm) and connected in series to a Betasil 5 μm 100 Å C_{18} HPLC column (21.2 × 150 mm). The column was eluted with a linear gradient from 100% H_2O to 100% MeOH at a flow rate of 9 mL min^{-1} for 60 minutes with fractions collected every min. This provided mixtures of related compounds throughout all HPLC fractions, including **68** and **69** in fraction 47. Reverse-phase HPLC fractions 25–52 were then combined (189 mg) and adsorbed onto diol-bonded silica and loaded to an HPLC cartridge (20 mm × 10 mm) and connected in series to a YMC-pack diol 5 μm 120 Å HPLC column (21.2 × 150 mm). The column was eluted with a linear gradient from 85% hexane/15% CH_2Cl_2 to 100% CH_2Cl_2 over 55 min, then to 90% CH_2Cl_2/10% MeOH over 20 min at a flow rate of 9 mL min^{-1} for 60 minutes with fractions collected every min, providing a mixture of **68** and **69** in fraction 10 (0.6 mg).

Data availability

The ESI file contains data used to develop the MW and D prediction models. The DEREP-NP database containing predicted D can be downloaded at https://github.com/guykl/.

Author contributions

Contributions to the preparation of this manuscript are as follows; GK: conceptualization, data curation, formal analysis, investigation, methodology, resources, validation, visualization, writing – original draft, writing – review & editing, DH: investigation, resources, writing – review & editing, JP: investigation, resources, AC: conceptualization, data curation, formal analysis, funding acquisition, investigation, methodology, project administration, resources, supervision, validation, visualization, writing – review & editing.

Conflicts of interest

There are no conflicts to declare.

Acknowledgements

We thank Frederic Leusch for providing several compounds used to establish calibration curve. We thank Wendy Loa-Kum-Cheung for her assistance with NMR data acquisition.

Notes and references

‡ The DEREP-NP database in DataWarrior format (dwr) with predicted D can be downloaded at https://github.com/guykl/.

1 M. S. Butler, *J. Nat. Prod.*, 2004, **67**, 2141–2153.

2 M. Wang, J. J. Carver, V. V. Phelan, L. M. Sanchez, N. Garg, Y. Peng, D. D. Nguyen, J. Watrous, C. A. Kapono, T. Luzzatto-Knaan, C. Porto, A. Bouslimani, A. V. Melnik, M. J. Meehan, W. T. Liu, M. Crüsemann, P. D. Boudreau, E. Esquenazi, M. Sandoval-Calderón, R. D. Kersten, L. A. Pace, R. A. Quinn, K. R. Duncan, C. C. Hsu, D. J. Floros, R. G. Gavilan, K. Kleigrewe, T. Northen, R. J. Dutton, D. Parrot, E. E. Carlson, B. Aigle, C. F. Michelsen, L. Jelsbak, C. Sohlenkamp, P. Pevzner, A. Edlund, J. McLean, J. Piel, B. T. Murphy, L. Gerwick, C. C. Liaw, Y. L. Yang, H. U. Humpf, M. Maansson, R. A. Keyzers, A. C. Sims, A. R. Johnson, A. M. Sidebottom, B. E. Sedio, A. Klitgaard, C. B. Larson, C. A. P. Boya, D. Torres-Mendoza, D. J. Gonzalez, D. B. Silva, L. M. Marques, D. P. Demarque, E. Pociute, E. C. O'Neill, E. Briand, E. J. N. Helfrich, E. A. Granatosky, E. Glukhov, F. Ryffel, H. Houson, H. Mohimani, J. J. Kharbush, Y. Zeng, J. A. Vorholt, K. L. Kurita, P. Charusanti, K. L. McPhail, K. F. Nielsen, L. Vuong, M. Elfeki, M. F. Traxler, N. Engene, N. Koyama, O. B. Vining, R. Baric, R. R. Silva, S. J. Mascuch, S. Tomasi, S. Jenkins, V. Macherla, T. Hoffman, V. Agarwal, P. G. Williams, J. Dai, R. Neupane, J. Gurr, A. M. C. Rodríguez, A. Lamsa, C. Zhang, K. Dorrestein, B. M. Duggan, J. Almaliti, P. M. Allard, P. Phapale, L. F. Nothias, T. Alexandrov, M. Litaudon, J. L. Wolfender, J. E. Kyle, T. O. Metz, T. Peryea, D. T. Nguyen, D. VanLeer, P. Shinn, A. Jadhav, R. Müller, K. M. Waters, W. Shi, X. Liu, L. Zhang, R. Knight, P. R. Jensen, B. Palsson, K. Pogliano,

R. G. Linington, M. Gutiérrez, N. P. Lopes, W. H. Gerwick, B. S. Moore, P. C. Dorrestein and N. Bandeira, *Nat. Biotechnol.*, 2016, **34**, 828–837.
3 J. Y. Yang, L. M. Sanchez, C. M. Rath, X. Liu, P. D. Boudreau, N. Bruns, E. Glukhov, A. Wodtke, R. De Felicio, A. Fenner, W. R. Wong, R. G. Linington, L. Zhang, H. M. Debonsi, W. H. Gerwick and P. C. Dorrestein, *J. Nat. Prod.*, 2013, **76**, 1686–1699.
4 A. T. Aron, E. C. Gentry, K. L. McPhail, L. F. Nothias, M. Nothias-Esposito, A. Bouslimani, D. Petras, J. M. Gauglitz, N. Sikora, F. Vargas, J. J. J. van der Hooft, M. Ernst, K. Bin Kang, C. M. Aceves, A. M. Caraballo-Rodríguez, I. Koester, K. C. Weldon, S. Bertrand, C. Roullier, K. Sun, R. M. Tehan, C. A. Boya P, M. H. Christian, M. Gutiérrez, A. M. Ulloa, J. A. Tejeda Mora, R. Mojica-Flores, J. Lakey-Beitia, V. Vásquez-Chaves, Y. Zhang, A. I. Calderón, N. Tayler, R. A. Keyzers, F. Tugizimana, N. Ndlovu, A. A. Aksenov, A. K. Jarmusch, R. Schmid, A. W. Truman, N. Bandeira, M. Wang and P. C. Dorrestein, *Nat. Protoc.*, 2020, **15**, 1954–1991.
5 J. Hubert, J. M. Nuzillard and J. H. Renault, *Phytochem. Rev.*, 2017, **16**, 55–95.
6 K. Scheubert, F. Hufsky, D. Petras, M. Wang, L. Nothias, K. Dührkop, N. Bandeira, P. C. Dorrestein and S. Böcker, *Nat. Commun.*, 2017, **8**, 1494.
7 O. Corcoran and M. Spraul, *Drug Discovery Today*, 2003, **8**, 624–631.
8 O. Gökay and K. Albert, *Anal. Bioanal. Chem.*, 2012, **402**, 647–669.
9 C. L. Zani and A. R. Carroll, *J. Nat. Prod.*, 2017, **80**, 1758–1766.
10 L. Buedenbender, L. J. Habener, T. Grkovic, D. İ. Kurtböke, S. Duffy, V. M. Avery and A. R. Carroll, *J. Nat. Prod.*, 2018, **81**, 957–965.
11 R. Reher, H. W. Kim, C. Zhang, H. H. Mao, M. Wang, L.-F. Nothias, A. M. Caraballo-Rodriguez, E. Glukhov, B. Teke, T. Leao, K. L. Alexander, B. M. Duggan, E. L. Van Everbroeck, P. C. Dorrestein, G. W. Cottrell and W. H. Gerwick, *J. Am. Chem. Soc.*, 2020, **142**, 4114–4120.
12 J. M. Egan, J. A. van Santen, D. Y. Liu and R. G. Linington, *J. Nat. Prod.*, 2021, **84**, 1044–1055.
13 T. D. W. Claridge, *High-Resolution NMR Techniques in Organic Chemistry*, Elsevier, Boston, 3rd edn, 2016.
14 D. Li, G. Kagan, R. Hopson and P. G. Williard, *J. Am. Chem. Soc.*, 2009, **131**, 5627–5634.
15 R. Neufeld and D. Stalke, *Chem. Sci.*, 2015, **6**, 3354–3364.
16 M. Nilsson, M. A. Connell, A. L. Davis and G. A. Morris, *Anal. Chem.*, 2006, **78**, 3040–3045.
17 M. Nilsson and G. A. Morris, *Magn. Reson. Chem.*, 2006, **44**, 655–660.
18 M. Nilsson, A. M. Gil, I. Delgadillo and G. A. Morris, *Chem. Commun.*, 2005, 1737–1739.
19 G. Dal Poggetto, L. Castañar, M. Foroozandeh, P. Kiraly, R. W. Adams, G. A. Morris and M. Nilsson, *Anal. Chem.*, 2018, **90**, 13695–13701.
20 M. Foroozandeh, L. Castañar, L. G. Martins, D. Sinnaeve, G. D. Poggetto, C. F. Tormena, R. W. Adams, G. A. Morris and M. Nilsson, *Angew. Chem., Int. Ed.*, 2016, **55**, 15579–15582.
21 A. Chen, D. Wu and C. S. Johnson, *J. Am. Chem. Soc.*, 1995, **117**, 7965–7970.
22 W. Li, H. Chung, C. Daeffler, J. A. Johnson and R. H. Grubbs, *Macromolecules*, 2012, **45**, 9595–9603.
23 D. Li, I. Keresztes, R. Hopson and P. G. Williard, *Acc. Chem. Res.*, 2009, **42**, 270–280.
24 R. T. Williamson, E. L. Chapin, A. W. Carr, J. R. Gilbert, P. R. Graupner, P. Lewer, P. McKamey, J. R. Carney and W. H. Gerwick, *Org. Lett.*, 2000, **2**, 289–292.
25 M. Tsuda, T. Yasuda, E. Fukushi, J. Kawabata, M. Sekiguchi, J. Fromont and J. Kobayashi, *Org. Lett.*, 2006, **8**, 4235–4238.
26 J. A. Jones, D. K. Wilkins, L. J. Smith and C. M. Dobson, *J. Biomol. NMR*, 1997, **10**, 199–203.
27 M. Feher and J. M. Schmidt, *J. Chem. Inf. Comput. Sci.*, 2003, **43**, 218–227.
28 S. Augé, P. Schmit, C. A. Crutchfield, M. T. Islam, D. J. Harris, E. Durand, M. Clemancey, A.-A. Quoineaud, J. Lancelin, Y. Prigent, F. Taulelle and M.-A. Delsuc, *J. Phys. Chem. B*, 2009, **113**, 1914–1918.
29 C. A. Crutchfield and D. J. Harris, *J. Magn. Reson.*, 2007, **185**, 179–182.
30 S. Bachmann, R. Neufeld, M. Dzemski and D. Stalke, *Chem.–Eur. J.*, 2016, **22**, 8462–8465.
31 E. J. Cabrita and S. Berger, *Magn. Reson. Chem.*, 2001, **39**, S142–S148.
32 G. S. Kapur, E. J. Cabrita and S. Berger, *Tetrahedron Lett.*, 2000, **41**, 7181–7185.
33 M. H. Abraham, P. L. Grellier, D. V Prior, P. P. Duce, J. J. Morris and P. J. Taylor, *J. Chem. Soc., Perkin Trans. 2*, 1989, 699.
34 M. H. Abraham, *Chem. Soc. Rev.*, 1993, **22**, 73.
35 M. H. Abraham, R. J. Abraham, J. Byrne and L. Griffiths, *J. Org. Chem.*, 2006, **71**, 3389–3394.
36 M. H. Abraham, P. P. Duce, J. J. Morris and P. J. Taylor, *J. Chem. Soc., Faraday Trans. 1*, 1987, **83**, 2867–2881.
37 S. P. D. Senadeera, L. Lucantoni, S. Duffy, V. M. Avery and A. R. Carroll, *J. Nat. Prod.*, 2018, **81**, 1588–1597.
38 A. K. Kreyenschmidt, S. Bachmann, T. Niklas and D. Stalke, *ChemistrySelect*, 2017, **2**, 6957–6960.
39 S. P. D. Senadeera, S. Duffy, V. M. Avery and A. R. Carroll, *Bioorg. Med. Chem. Lett.*, 2017, **27**, 2602–2607.
40 P. S. Pregosin, *Prog. Nucl. Magn. Reson. Spectrosc.*, 2006, **49**, 261–288.
41 E. J. Cabrita and S. Berger, *Magn. Reson. Chem.*, 2002, **40**, S122–S127.
42 A. Harvey, R. Edrada-Ebel and R. J. Quinn, *Nat. Rev. Drug Discovery*, 2015, **14**, 111–129.
43 K. Valkó, C. Bevan and D. Reynolds, *Anal. Chem.*, 1997, **69**, 2022–2029.
44 C. M. Du, K. Valko, C. Bevan, D. Reynolds and M. H. Abraham, *J. Liq. Chromatogr. Relat. Technol.*, 2001, **24**, 635–649.
45 T. Sander, J. Freyss, M. von Korff and C. Rufener, *J. Chem. Inf. Model.*, 2015, **55**, 460–473.
46 R. C. Bowyer and P. R. Jefferies, *Chem. Ind.*, 1963, 1245–1246.
47 R. E. Corbett and R. N. Speden, *J. Chem. Soc.*, 1958, 3710–3715.
48 G. Kleks, D. C. Holland, E. K. Kennedy, V. M. Avery and A. R. Carroll, *J. Nat. Prod.*, 2020, **83**, 3435–3444.